



ARCHIVES  
of  
FOUNDRY ENGINEERING

ISSN (2299-2944)  
Volume 21  
Issue 1/2021

101 – 112

10.24425/afe.2021.136085

15/1



Published quarterly as the organ of the Foundry Commission of the Polish Academy of Sciences

# Free Vibration Analysis of A357 Alloy Reinforced with Dual Particle Size Silicon Carbide Metal Matrix Composite Plates Using Finite Element Method

A. Lakshmikanthan <sup>a, b</sup>, V. Mahesh <sup>c</sup>, R. T. Prabhu <sup>d</sup>,  
M. G. C. Patel <sup>e</sup>, S. Bontha <sup>a, \*</sup>

<sup>a</sup> Department of Mechanical Engineering, National Institute of Technology Karnataka, Surathkal, Mangalore-575025, Karnataka, India

<sup>b</sup> Department of Mechanical Engineering, Nitte Meenakshi Institute of Technology, Bangalore, India-560064

<sup>c</sup> Nonlinear Multifunctional Composites Analysis and Design (NMCAD) Laboratory, Department of Aerospace Engineering, Indian Institute of Science, Bangalore, India-560012

<sup>d</sup> CEMILAC, Defence R&D Organisation, Bangalore, India-560093

<sup>e</sup> Department of Mechanical Engineering, PES Institute of Technology and Management, Shivamogga, India-577204

\* Corresponding author. E-mail address: srikanth.bontha@nitk.edu.in

Received 30.11.2020; accepted in revised form 15.02.2021

## Abstract

In this work, the free vibration behaviour of A357 composite plate reinforced with dual particle size (DPS) (3 wt.% coarse + 3 wt.% fine, 4 wt.% coarse + 2 wt.% fine, and 2 wt.% coarse + 4 wt.% fine) SiC is evaluated using the finite element method. To this end, first-order shear deformation theory (FSDT) has been used. The equations of motion have been derived using Hamilton's principle and the solution has been obtained through condensation technique. A thorough parametric study was conducted to understand the effect of reinforcement size and weight fraction, boundary conditions, aspect ratio and length-to-width ratio of plate geometry on natural frequencies of A357/DPS-SiC composite plates. Results reveal significant influence of all the above variables on natural frequency of the composite plates. In all the cases, A357 composite plate reinforced with 4 wt.% coarse and 2 wt.% fine SiC particles displayed the highest natural frequency owing to its higher elastic and rigidity modulus. Further, the natural frequencies increase with decrease in aspect ratio of the plate geometry. Natural frequency also decreases with increase in the number of free edges. Lastly, increasing the length-to-width ratio drastically improves the natural frequency of the plates.

**Keywords:** Finite element method, First order shear deformation theory (FSDT), A357 alloy, Hamilton's principle, A357/DPS-SiC Composites

## 1. Introduction

Aluminium alloys and their composites find applications in aerospace, marine and electrical industries due to their high strength-to-weight ratio [1], corrosion [2] and wear resistance [3-4]. To meet industrial requirements, the developed composite materials should have better performance in both static and dynamic conditions. Presently, several researchers have investigated composite structures for damping and vibrational properties using finite element methods [5]. Researchers have modelled the composite structures as a plate, which has different vibrational characteristics. Determining natural frequency is one of the most important requirements for designing machine structures that are subjected to complicated external dynamic loading conditions. Generally, high strength and stiffness materials have low damping properties. To increase the damping properties of high strength materials reinforcements are added. The addition of reinforcements increases the damping properties of both the matrix as well as that of the composites. Initially, the laminate theory was used to predict damping values of composites from the relative volume fraction of matrix and reinforcements as a function of frequency and operating temperature [5]. Further, this model could be used to monitor the degradation of mechanical strength of reinforcements due to processing [6]. During the process, the composite materials relaxed due to the reorientation of matrix and reinforcement pairs. Experimental results reveal that no significant change in damping occurs due to thermo elastic transport effect [7]. The classical model theory postulated that dynamic dislocation density formed due to high residual stresses can enhance damping properties [8]. The theoretical model showed that peak damping is attained for the low volume fraction of composites because of interfacial slip caused due to imperfect bonding [9]. Critical damping is strongly influenced by the friction coefficient between the constituents of the composite [10]. Apart from microstructural and mechanical properties, it is believed that the structural properties of A357 alloy and its composites should be enhanced. To enhance these properties high damping materials should be added as reinforcements. Materials with high damping can dissipate mechanical energy, are capable of noise control and can attenuate wave propagation [11-13]. Discontinuous reinforcements such as SiC can significantly affect the attenuating characteristics of metal matrix composite plates [14-16]. Eruslu and Aydogdu [17] investigated the frequency characteristics of Al/SiC composite plates using classical plate theory. Ei-Kady et al. [18] analysed the dynamic response of aluminium metal matrix nano-composites through frequency response and damping factors. Both, experimental and theoretical studies have shown that addition of ceramic reinforcements to the Al matrix leads to enhancement in the stiffness of the composites even during dynamic conditions.

Raju and Reddy [19] studied the effect of mechanical properties and frequency response characteristics of SiC/glass fiber and graphene/glass fiber reinforced epoxy composites by applying simply supported and free edge boundary conditions. The response of these composites were compared with the results obtained for SiC/graphene/glass fiber reinforced epoxy hybrid composite. Soleymani and Asghari [20] investigated the effect of particle size, shape, and orientation on Al/SiC composite using

the finite element method. They reported that the shape and orientation of particles influenced the stress homogeneity. Further, it was also reported that the size distribution has the least effect on the composite. Numanoglu et al. [21] investigated stability analysis of SiC and boron nitride (BN) nanotubes/nanowires by using different size effective theories and FE methods. Khan et al. [22] developed a FE model for free vibration and static response of Al/SiC and Ni/Al<sub>2</sub>O<sub>3</sub> functionally graded materials (FGM's). FE model results showed that the natural frequencies obtained from these two FGM's were in line with those published in the literature. Zuo et al. [23] used two-dimensional finite element based Mindlin plate theory for the study of free vibration, bending and buckling analysis of Al/SiC, Al/Al<sub>2</sub>O<sub>3</sub> and Al/Si<sub>3</sub>N<sub>4</sub> FGM plates. They reported that the wavelet FEM method was found to be an efficient and accurate tool for solving the FGM structures. Xizhong et al. [24] studied the effect of initial packing structure, external pressure with SiC content on packing densification for 2D-Al/SiC core/shell composite powders using discrete element method (DEM-FEM) as well as multi-particle element method (MPFEM). Bozkurt and Ersoy [25] studied the vibration behavior of Al2124/SiC composites plate using FEM. Their work revealed that the natural and modal frequency range was consistent throughout the composite plate. Santhosh et al. [26] studied the vibration characteristics of Al5083 reinforced with fly ash and SiC using fast fourier transformation (FFT) analysis. Results showed that the composite with 2% of flyash and 9% SiC displayed better damping characteristics. Kushwaha and Vimal [27] studied the vibrational analysis of laminated composite plates using FE method. The influence of various parameters such as boundary conditions, aspect ratios, and fiber orientation of laminated composites on the natural frequency was assessed. The non-dimensional frequency was found to decrease with an increase in thickness to width ratio and increase with an increase in the angle of orientation of fibers. Kenneth and Adetomilola [28] studied the damping behavior of steel, steel/graphite, and SiC reinforced Al-Mg-Si matrix-based composites. Results reveal that higher damping capacity was achieved for the composite reinforced with 8% SiC content. Gholami and Ansari [29] studied the free vibration characteristics of post-buckled functionally graded carbon nanotube (FG-CNT) annular plates. By using Hamilton's principle, a nonlinear equation was derived, and finally, the effects of different parameters like volume fraction, thickness (inner and outer) were analyzed. Very recently, the effectiveness of FE methods in predicting the natural frequencies of smart composite plates was demonstrated by Vinyas and co-researchers [30-32].

Limited work has been reported in literature with regards to developing an effective model for determining the structural properties of composite materials using different micromechanical approaches. Therefore, in this work, an attempt has been made to evaluate the stiffness characteristics of A357/DPS-SiC composite plates. To this end, a finite element formulation has been derived under the framework of first-order shear deformation theory (FSDT).

## 2. Fabrication details and material properties of A357/DPS-SiC composite plates

This work focuses on understanding the free vibration behavior of the A357/DPS-SiC composite plates using finite element method. There is no experimental work being reported herein. However, for the benefit of the reader, a brief overview is provided below regarding the material and its properties used in the computational modeling work along with reference to the authors prior work.

The materials used in this study are A357 (matrix material) and SiCp (reinforcement material) of two different mesh sizes: Coarse ( $140 \pm 10 \mu\text{m}$ ) and Fine ( $30 \pm 5 \mu\text{m}$ ). Stir casting method was used to produce the DPS composites and has been described in detail in the prior work of authors [33,34]. The micron-sized SiC particles generally exhibited angular morphology. However, there were also a few particles that exhibited irregular shaped morphology. The authors in their prior work reported enhanced properties (strength, hardness, and wear resistance) with the above particle size and morphology [35]. The material properties of A357 alloy and SiCp are given below in Table 1.

Table 1.  
Properties of A357 alloy and Silicon Carbide [36].

Material	Elastic Modulus E (GPa)	Poisson's ratio ( $\nu$ )	Shear Modulus G (GPa)
A357 alloy	72.4	0.33	26.8
SiC	410	0.14	180

## 3. Modeling framework

### 3.1. Displacement equations

The three displacement components ( $u$ ,  $v$  and  $w$ ) of the plate are assumed to follow FSDT (Fig. 1.) as follows [37]:

$$\begin{aligned} u &= u_0 + z\theta_x \\ v &= v_0 + z\theta_y \\ w &= w_0 \end{aligned} \quad (1)$$

Where,  $u_0, v_0$  and  $w_0$  denote the displacements (mid-plane) along  $x$ ,  $y$  and  $z$  axes respectively.  $\theta_x$  and  $\theta_y$  are the rotations of the portions of the normal lying in the  $xz$  plane and  $yz$  plane, respectively. Also,  $t$  denotes thickness of the laminate. The reference plane ( $z = 0$ ) is chosen at the mid-plane of the laminate.

The bending strains can be expressed as follows [37]:

$$\{\varepsilon_b\} = [B_{tb}] \{d_t^e\} + z [B_{rb}] \{d_r^e\} \quad (2)$$

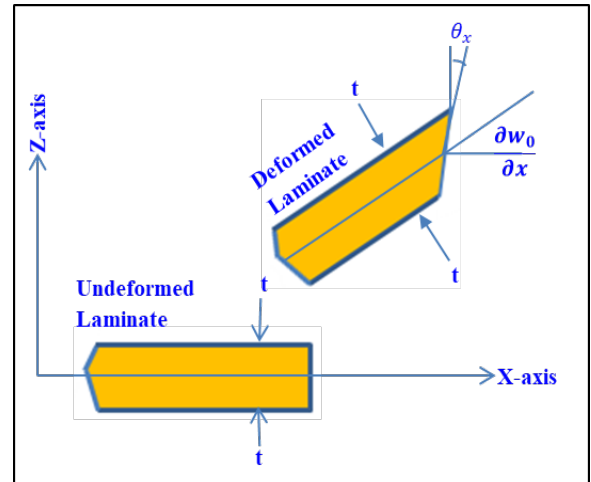


Fig. 1. First-order shear deformation theory (FSDT) [38]

In a similar way, the shear strains can be expressed as follows [37]:

$$\{\varepsilon_s\} = [B_{ts}] \{d_t^e\} + [B_{rs}] \{d_r^e\} \quad (3)$$

In equations (2) and (3),  $[B_{tb}]$ ,  $[B_{rb}]$ ,  $[B_{ts}]$  and  $[B_{rs}]$  are the different strain-displacement matrices which are defined as follows [36]:

$$\begin{aligned} [B_{tb}] &= \begin{bmatrix} N_{i,x} & 0 & 0 \\ 0 & N_{i,y} & 0 \\ N_{i,y} & N_{i,x} & 0 \end{bmatrix}, \quad [B_{rb}] = \begin{bmatrix} N_{i,x} & 0 \\ 0 & N_{i,y} \\ N_{i,y} & N_{i,x} \end{bmatrix} \\ [B_{ts}] &= \begin{bmatrix} 0 & 0 & N_{i,x} \\ 0 & 0 & N_{i,y} \end{bmatrix}, \quad [B_{rs}] = \begin{bmatrix} 1 & 0 \\ 0 & 1 \end{bmatrix} \end{aligned} \quad (4)$$

### 3.2. Finite element formulation

Using an 8 noded isoparametric element, the finite element model for composite plate is generated. The generalized degrees of freedom (DOF) of the element can be represented as [37],

$$\begin{aligned} \{d_{ii}\} &= [u_i \ v_i \ w_i]^T, \quad \{d_{ri}\} = [\theta_x \ \theta_y]^T \\ \{d_t\} &= [N_t] \{d_t^e\}, \quad \{d_r\} = [N_r] \{d_r^e\} \end{aligned} \quad (5)$$

Where  $\{d_t\}$  is the translational displacement vector and  $\{d_r\}$  is the rotational vector. Further,  $\{d_{ti}\}$  and  $\{d_{ri}\}$  are the displacement and rotational vectors associated with the  $i^{\text{th}}$  ( $i = 1, 2, 3 \dots 8$ ) node of the element [37].

### 3.3. Equations of motion

The governing equations of motion for A357/DPS-SiC composite plates can be represented using the first variations of total potential energy  $T_p$  and kinetic energy  $T_k$  of the typical element as follows [39, 40]:

$$\delta T_p = \frac{1}{2} \sum_{n=1}^N \int_{\Omega^n} \delta \{\varepsilon_b\}^T \{\sigma_b\} d\Omega^n + \frac{1}{2} \sum_{n=1}^N \int_{\Omega^k} \delta \{\varepsilon_s\}^T \{\sigma_s\} d\Omega^n$$

$$\delta T_k = \int_{\Omega^n} \delta \{d_t\} \rho \{\ddot{d}_t\} d\Omega^n \quad (6)$$

In equation 6, “ $n$ ” denotes layer number and “ $\Omega$ ” denotes volume of the  $n^{\text{th}}$  layer. Further application of Hamilton’s principle to A357/DPS-SiC composite plates is as follows [39, 40].

$$\delta T_p + \delta T_k = 0 \quad (7)$$

The fundamental equilibrium equations of motion are as given below [38, 39]. In equation 8,  $[M_{tt}^e]$  and  $[K_{tt}^e]$ ,  $[K_{tr}^e]$ ,  $[K_{rr}^e]$  denote mass matrix and elastic stiffness matrices respectively.

$$\left[ M_{tt}^e \right] \left\{ \ddot{d}_t^e \right\} + \left[ K_{tt}^e \right] \left\{ d_t^e \right\} + \left[ K_{tr}^e \right] \left\{ d_r^e \right\} = 0$$

$$\left[ K_{tr}^e \right]^T \left\{ d_t^e \right\} + \left[ K_{rr}^e \right] \left\{ d_r^e \right\} = 0 \quad (8)$$

### 3.4. Boundary conditions

The free vibration behaviour of A357/DPS-SiC composite plates have been studied using the finite element formulation presented in the preceding section. The geometrical dimensions of the composite plate selected are as follows: length  $a = 1\text{m}$ , width  $b = 1\text{m}$  and thickness  $h = 0.3\text{m}$ . The composition of A357/DPS-SiC composites and their material properties, i.e., Young’s modulus ( $E$ ), Poisson’s ratio ( $\nu$ ) and Shear modulus ( $G$ ) which were computed using the extended rule of mixtures [29, 40,41,42] are tabulated in Tables 2 and 3 respectively.

Further, the influence of parameters such as boundary conditions, length-to-width ratio, and aspect ratio on frequency response have been studied in detail. The A357/DPS-SiC composite plate geometry, boundary conditions chosen for both the simply supported and clamped conditions are shown in Figs. 2. and 3, respectively.

Clamped edge (C):

$$u = v = w = \theta_x = \theta_y = 0 \quad (9)$$

Free edge (F):

$$u = v = w = \theta_x = \theta_y \neq 0 \quad (10)$$

Simply supported edge (S):

$$u = \theta_x \neq 0; v = w = 0 \text{ at } x = 0, a$$

$$v = \theta_y \neq 0; u = w = 0 \text{ at } y = 0, b \quad (11)$$

Table 2.

Composition of A357/DPS-SiC composite plates [34]

Base alloy Composition (%)	Quantity of Reinforcement Weight percentage (Wt. %) added	Ratio of Coarse ( $140 \pm 10\mu\text{m}$ ) and Fine ( $30 \pm 5 \mu\text{m}$ ) size SiC Particles	Alloy/Composite Designation
100	0	0:0 (Nil)	A357 alloy
94	6	3:3 ( Coarse : Fine)	DPS-1 composite
94	6	4:2 ( Coarse : Fine )	DPS-2 composite
94	6	2:4 ( Coarse : Fine )	DPS-3 composite

Table 3.

Material properties of A357/DPS-SiC composite plates

Designation	Elastic Modulus E (GPa)	Poisson’s ratio ( $\nu$ )	Shear Modulus G (GPa)
A357 alloy [36]	72.4	0.33	26.8
DPS-1 composite	82.66	0.29	29.54
DPS-2 composite	85.95	0.29	30.12
DPS-3 composite	77.89	0.28	28.92

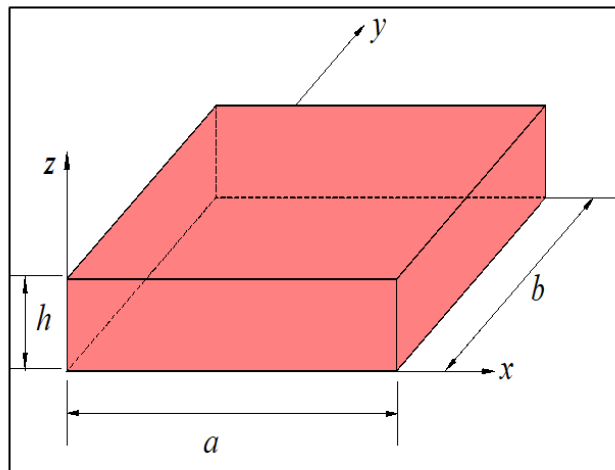


Fig. 2. A357/DPS-SiC composite plate geometry

### 3.5. Convergence and verification studies

A convergence study was carried out to evaluate the stability of the finite element formulation considered herein. In this regard, the natural frequencies of the A357/DPS-SiC composite plates were calculated and the results were compared with that reported by Klimenda and Soukup [43]. The results of the convergence study indicate that a mesh size of  $10 \times 10$  is good enough for obtaining natural frequencies with high degree of accuracy. Therefore, all subsequent analysis have been carried out with a mesh size of  $10 \times 10$ . Further, the credibility of the proposed finite element formulation is verified by comparing the results from the present study with that of the results reported by Klimenda and Soukup [43].

For this purpose of verification, the geometrical dimensions and the material properties are analogous to that used by Klimenda and Soukup [43] in their study. It can be noticed from Table 4 and Fig.4. that the results reported herein match well with that of Klimenda and Soukup [43]. it can be concluded that the present finite element formulation yields accurate results, and it can be extended to carry out the frequency response analysis of A357/DPS-SiC composite plates.

## 4. Results and Discussion

### 4.1. Effect of reinforcement

In this section, the influence of size and different weight fraction of reinforcement of SiC (3% coarse + 3% fine, 4% coarse + 2% fine, and 2% coarse + 4% fine) on the natural frequencies of A357/DPS-SiC composite plates is presented. To this end, the material properties presented in Table 3 are used for evaluation. The results of Table 5 affirm that the plates made of DPS-2 composite yield a higher frequency, followed by that of DPS-1 and DPS-3 composites. This can be attributed to the fact that DPS-2 composite has a higher Elastic (E) and Rigidity modulus (G) when compared to DPS-1 and DPS-3 composites. In contrast, the effect of poisson's ratio is minimal when compared to that of E and G.

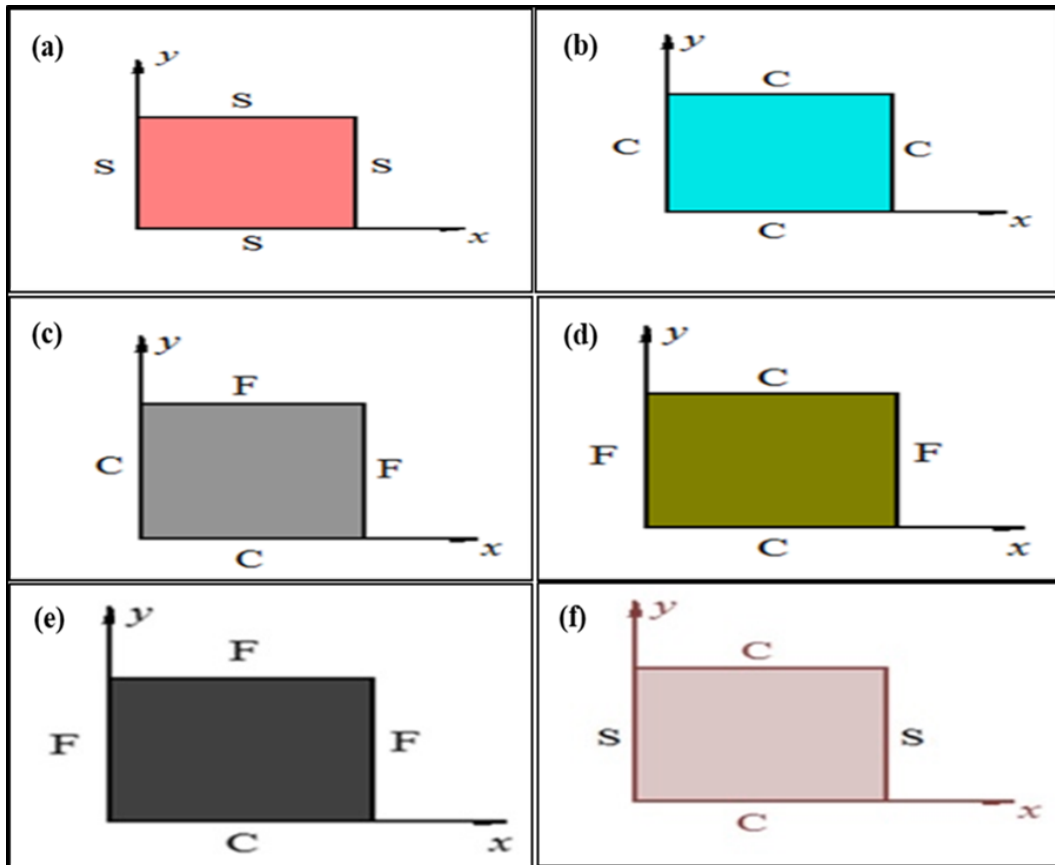


Fig. 3. Schematic of various boundary conditions applied on A357/DPS-SiC composite plate geometry: (a) All sides simply supported (SSSS) (b) All sides clamped (CCCC) (c) Adjacent sides clamped (CCFE) (d) Opposite sides clamped (CFCF) (e) One side clamped and rest free edges (CFFF) and (f) Two sides clamped and two sides simply supported (CSCS)

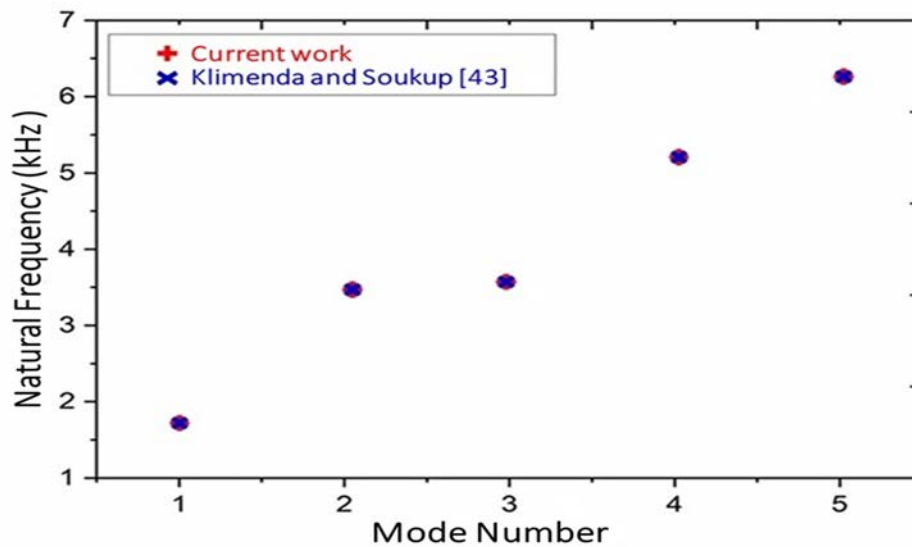


Fig. 4. Comparison of obtained Natural Frequencies with ones reported by Klimenda and Soukup [43]

Table 4.  
Verification of natural frequencies

Mode numbers	Mesh size				Klimenda and Soukup [43]
	4×4	6×6	8×8	10×10	
1	1745.4	1745.8	1746.2	1746.7	1744.4
2	3546.1	3546.8	3547.1	3547.8	3545.4
3	3546.1	3546.8	3547.1	3547.8	3545.4
4	5212.7	5213.6	5213.9	5214.2	5210.3
5	6325.8	6326.9	6327.0	6327.3	6324.9

#### 4.2. Effect of aspect ratio ( $a/h$ ratio)

The effect of aspect ratio on the frequency response of A357/DPS-SiC composite plates was evaluated by considering only two boundary conditions: all sides simply supported (SSSS) and all sides clamped (CCCC). It can be noticed from Figs. 5. and 6. that for A357 alloy and DPS composites, the natural frequencies are higher for lesser  $a/h$  ratio i.e., for thick plates. For the sake of

brevity, only first three natural frequencies have been depicted here.

The natural frequency of A357 alloy is lower compared to DPS composites. The plate made of DPS-2 composite yields a higher natural frequency, which are followed by DPS-1 and DPS-3 composites. This can be attributed to the fact that DPS-2 has a higher Elastic and Rigidity modulus when compared to DPS-1 and DPS-3 composites.

Table 5.  
Effect of reinforcement size and weight fraction on the natural frequency of A357/DPS-SiC composite plates

Natural Frequency ( $10^4 \text{ rad sec}^{-1}$ )							
A357 Alloy		DPS-1 Composite		DPS-2 Composite		DPS-3 Composite	
SSSS	CCCC	SSSS	CCCC	SSSS	CCCC	SSSS	CCCC
0.4719	0.8093	0.4804	0.8278	0.4917	0.8474	0.4717	0.8137
1.1302	1.4993	1.1542	1.5387	1.1815	1.5752	1.1342	1.5138
1.1302	1.4993	1.1542	1.5387	1.1815	1.5752	1.1342	1.5138
1.4382	1.9964	1.5068	2.0528	1.5425	2.1014	1.4898	2.0204
1.4382	2.2332	1.5068	2.2997	1.5425	2.3541	1.4898	2.2642
1.6864	2.2438	1.7261	2.3103	1.767	2.3649	1.697	2.2745
2.0166	2.5394	2.07	2.6168	2.119	2.6787	2.0365	2.5768
2.0166	2.5394	2.07	2.6168	2.119	2.6787	2.0365	2.5768
2.1897	2.8679	2.2936	2.9568	2.3478	3.0267	2.2676	2.9108
2.3982	2.8735	2.4661	2.9568	2.5244	3.0267	2.4272	2.9108

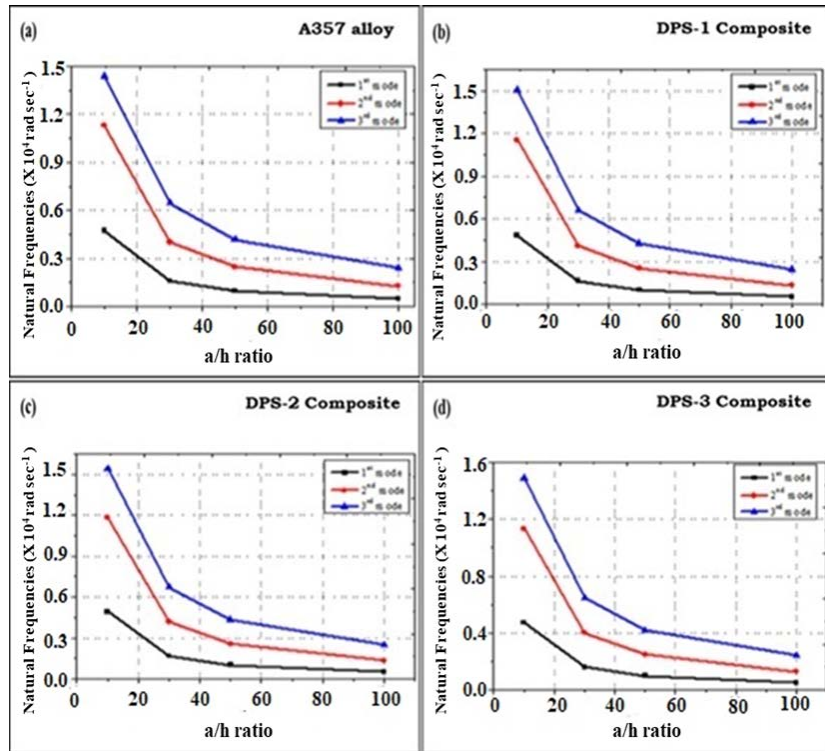


Fig. 5. Effect of aspect ratio ( $a/h$ ) on frequency response of A357/DPS-SiC composite plates with SSSS condition. (a) A357 Alloy, (b) DPS-1 Composite, (c) DPS-2 Composite and (d) DPS-3 Composite

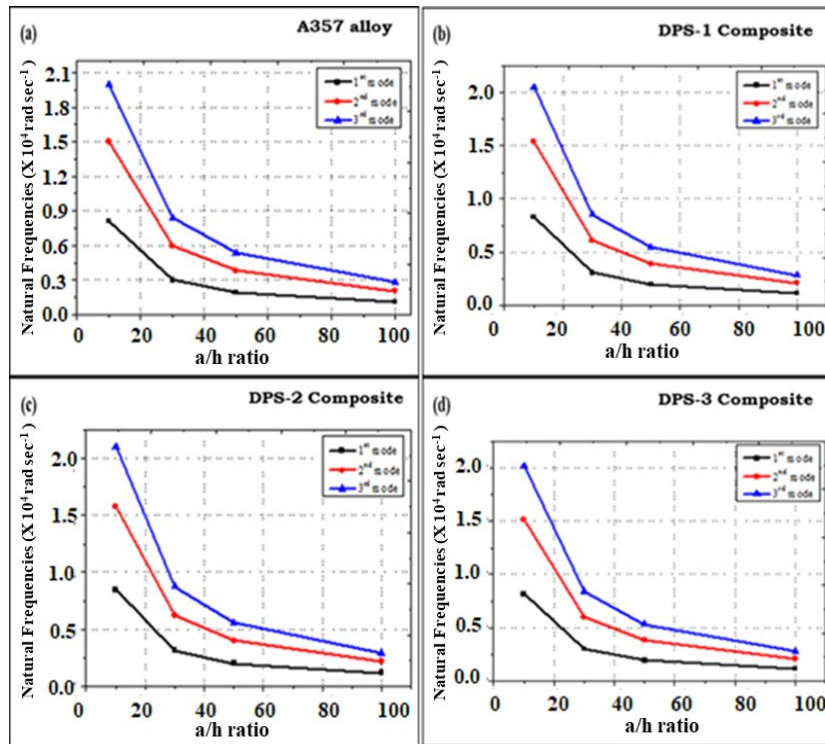


Fig. 6. Effect of aspect ratio ( $a/h$ ) on frequency response of A357/DPS-SiC composite plates with CCCC condition (a) A357 Alloy, (b) DPS-1 Composite, (c) DPS-2 Composite and (d) DPS-3 Composite

### 4.3. Effect of boundary conditions

The boundary conditions illustrated in Fig. 2. (Eqs. (9) – (11)) were enforced on the A357/DPS-SiC composite plates. Further, the effect of different combinations of boundary conditions were also investigated. From Table 6, it can be observed that for all the material compositions, the natural frequency reduces drastically with the increase in number of free edges. Next, asymmetric free edges (CCFF) have a prominent effect in this reduction in contrast to symmetric free edges (CFCF). This is due to the decrease in the

rigidity of the plate with increase in the number of asymmetric free edges, thereby resulting in a reduction of natural frequency. For all the boundary conditions the plate made of DPS-2 composite yields a higher natural frequency, followed by that of DPS-1 and DPS-3 composite plates. These results can again be attributed to the fact that DPS-2 composite has a higher Elastic and Rigidity modulus when compared to DPS-1 and DPS-3 composites. Next, the mode shapes of DPS-2 composite plate with different boundary conditions have been illustrated in Fig. 7. Here, the maximum deformation of the plate is represented using red color.

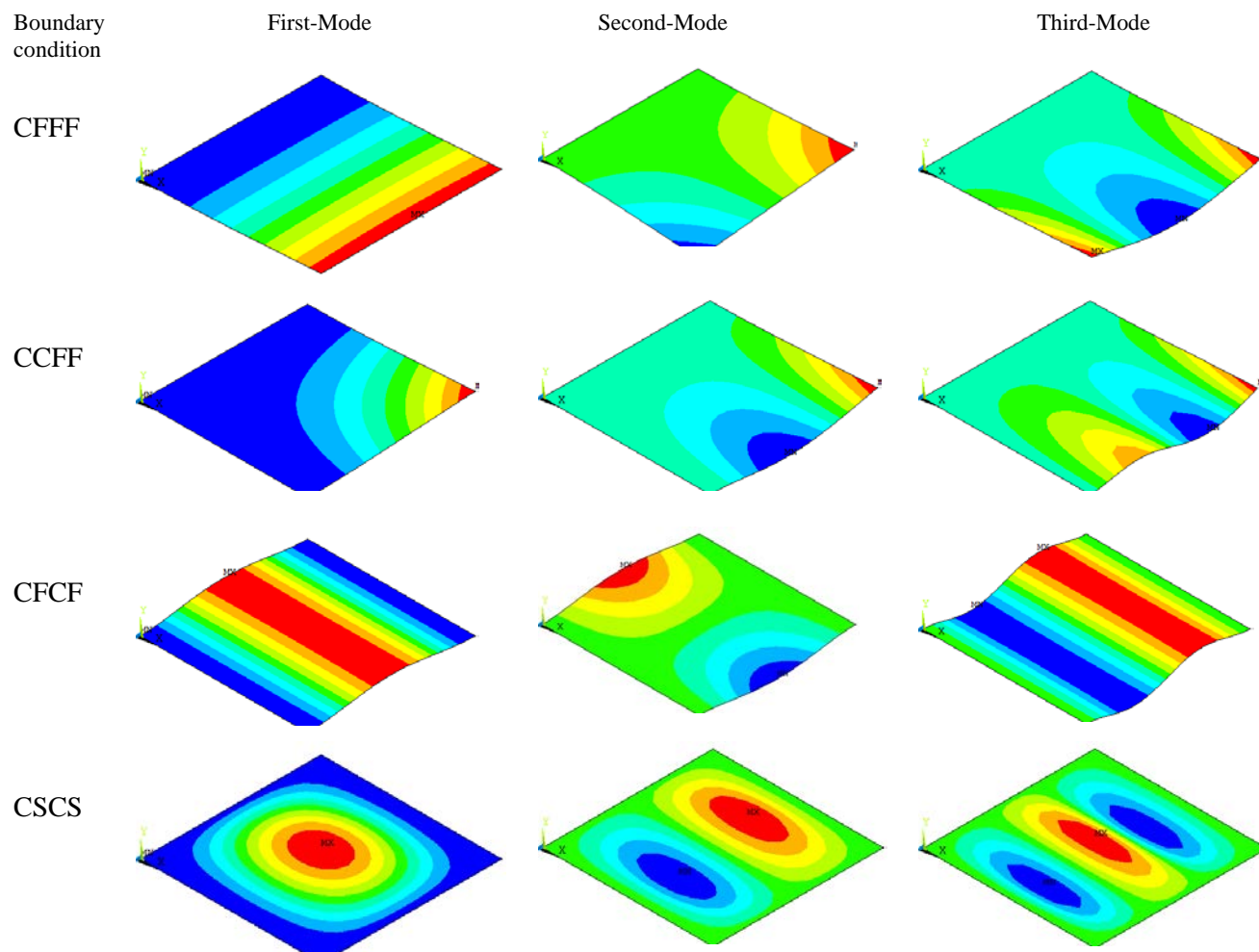


Fig. 7. Effect of boundary conditions on the first three mode shapes of DPS-2 Composite

Table 6.

Effect of boundary conditions on the first three natural frequencies of A357/DPS-SiC composite plates

Designation	Mode Number	Natural Frequency ( $10^3 \text{ rad sec}^{-1}$ )			
		CFCF	CCFF	CFFF	CSCS
A357 Alloy	1	0.5571	0.1645	0.0864	0.7646
	2	0.6206	0.5426	0.1904	1.6220
	3	1.0258	0.6388	0.4923	1.7873
DPS-1 Composite	1	0.5689	0.1695	0.0883	0.7803
	2	0.6379	0.5619	0.1979	1.6600
	3	1.0547	0.6532	0.5085	1.8232
DPS-2 Composite	1	0.5823	0.1735	0.0903	0.7988
	2	0.6530	0.5752	0.2026	1.6993
	3	1.0797	0.6686	0.5206	1.8663
DPS-2 Composite	1	0.5590	0.1669	0.0867	0.7667
	2	0.6278	0.5540	0.1953	1.6321
	3	1.0382	0.6420	0.5010	1.7911

#### 4.4. Effect of length-to-width ratio ( $a/b$ )

Tables 7 and 8 document the effect of length-to-width ratio ( $a/b$ ) on the natural frequencies of A357/DPS-SiC composite plates that were subjected to different boundary conditions. The results of tables 7 and 8 clearly illustrate that the natural frequency increases with an increase in the length-to-width ratio ( $a/b$ ). This is due to the

increase in the rigidity of the plates with an increase in the  $a/b$  ratio [40]. For the SSSS & CCCC conditions the plate made of DPS-2 composite yields a higher natural frequency, followed by that of DPS-1 and DPS-3 composite plates. These trends are analogous to the trends in results presented earlier for effect of reinforcement, effect of aspect ratio and effect of boundary conditions.

Table 7.

Effect of length-to-width ratio ( $a/b$ ) on the first three natural frequencies of A357/DPS-SiC composite plates (SSSS condition)

Designation	Mode number	Natural Frequency ( $10^3 \text{ rad sec}^{-1}$ )			
		$a/b = 0.5$	$a/b = 1$	$a/b = 2$	$a/b = 3$
A357 Alloy	1	0.3098	0.4891	1.229	2.467
	2	0.5472	1.2719	2.009	3.177
	3	0.8668	1.2719	3.252	4.202
DPS-1 Composite	1	0.3152	0.4972	1.250	2.511
	2	0.5590	1.2964	2.047	3.234
	3	0.8841	1.2964	3.316	4.278
DPS-2 Composite	1	0.3226	0.5090	1.280	2.570
	2	0.5723	1.3271	2.095	3.310
	3	0.9050	1.3271	3.395	4.379
DPS-3 Composite	1	0.3094	0.4880	1.227	2.465
	2	0.5494	1.2733	2.010	3.175
	3	0.8685	1.2733	3.258	4.201

Table 8.

Effect of length-to-width ratio ( $a/b$ ) on the first three natural frequencies of A357/DPS-SiC composite plates (CCCC condition)

Designation	Mode number	Natural Frequency ( $10^4 \text{ rad sec}^{-1}$ )			
		$a/b = 0.5$	$a/b = 1$	$a/b = 2$	$a/b = 3$
A357 Alloy	1	0.0692	0.1116	0.2566	0.5164
	2	0.0967	0.2064	0.3403	0.5531
	3	0.1126	0.2064	0.4215	0.6021
DPS-1 Composite	1	0.0707	0.1144	0.2618	0.5261
	2	0.0989	0.2106	0.3479	0.5643
	3	0.1148	0.2106	0.4304	0.6154
DPS-2 Composite	1	0.0724	0.1171	0.2680	0.5385
	2	0.1013	0.2156	0.3561	0.5777
	3	0.1175	0.2156	0.4406	0.6299
DPS-3 Composite	1	0.0695	0.1125	0.2571	0.5167
	2	0.0973	0.2069	0.3420	0.5544
	3	0.1128	0.2069	0.4229	0.6048

## 5. Conclusions

This article deals with evaluating the free vibration characteristics of A357/DPS-SiC composite plates using the finite element method under the framework of FSDT. Among the different compositions considered, the DPS-2 composite has a prominent effect on the natural frequency. The parametric studies reported herein confirm that thick plates yield higher natural frequencies. Further, it is noticed that increasing the value of length-to-width ratio drastically improves the natural frequency. Finally, as the number of asymmetric free edges increase the rigidity of the plate reduces considerably, which in turn affects the natural frequency of the A357/DPS-SiC composite plates.

## References

- [1] Raju R. S. S., Panigrahi, M.K., Ganguly R.I., & Srinivasa Rao G. (2019). Tribological behaviour of al-1100-coconut shell ash (CSA) composite at elevated temperature. *Tribology International*. 129, 55-66.
- [2] Bishop, J.E., & Kinra, V.K. (1995). Analysis of elastothermodynamic damping in particle-reinforced metal-matrix composites. *Metallurgical and Materials Transactions A*. 26(11), 2773-2783.
- [3] Challer, R.S. (2003). Metal matrix composites, a smart choice for high damping materials. *Journal of Alloys and Compounds*. 355(1-2), 131-135.
- [4] Ehsani, R., & Seyed Reihani, S.M. (2004). Aging behaviour and tensile properties of squeeze cast Al 6061/SiC metal matrix composites. *Scientia Iranica*. 11(4), 392-397.
- [5] Zhang, J., Perez, R.J., Wong, C.R., & Lavernia, E.J. (1994). Effects of secondary phases on the damping behaviour of metals, alloys and metal matrix composites. *Materials Science and Engineering: R: Reports*. 13 (8), 325-389.
- [6] Lavernia, E.J., Perez, R.J., & Zhang, J. (1995). Damping behavior of discontinuously reinforced ai alloy metal-matrix composites. *Metallurgical and Materials Transactions A*. 26 (11), 2803-2818.
- [7] Wang, J., Li, Z., Fan, G., Pan, H., Chen, Z., & Zhang, D. (2012). Reinforcement with graphene nanosheets in aluminum matrix composites. *Scripta Materialia*. 66(8), 594-597.
- [8] Qian, L. F., Batra, R. C., & Chen, L. M. (2004). Static and dynamic deformations of thick functionally graded elastic plates by using higher-order shear and normal deformable plate theory and meshless local Petrov-Galerkin method. *Composites Part B: Engineering*. 35(6-8), 685-697.
- [9] Sharma, S.C., Krishna, M., & Narasimha Murthy, H.N. (2004). Studies on the effect of residual thermal stresses on thermal expansion and damping behaviour of Al6061/ALBITE MMCs. *Adv. in Vibration Engg.*, 3(4), 320-331 (2004).
- [10] Sastry, S., Krishna, M., & Uchil, J. (2001). A study on damping behaviour of aluminite particulate reinforced ZA-27 alloy metal matrix composites. *Journal of Alloys and Compounds*. 314(1-2), 268-274.
- [11] Zhang, J., Perez, R.J., Wong, C.R., & Lavernia, E.J. (1994). Effects of secondary phases on the damping behaviour of metals, alloys and metal matrix composites. *Materials Science and Engineering: R: Reports*. 13(8), 325-389.
- [12] James, D.W. (1969). High damping metals for engineering applications. *Materials Science and Engineering*. 4(1), 1-8.
- [13] Zhang, J., Perez, R.J., & Lavernia, E.J. (1993). Documentation of damping capacity of metallic, ceramic and metal-matrix composite materials. *Journal of Materials Science*. 28(9), 2395-2404.
- [14] Zhang, J., Perez, R.J., & Lavernia, E.J. (1994). Effect of SiC and graphite particulates on the damping behavior of metal matrix composites. *Acta Metallurgica et Materialia*. 42(2), 395-409.
- [15] Kang, C.S., Maeda, K., Wang, K.J., & Wakashima, K. (1998). Dynamic Young's modulus and internal friction in particulate SiC Al composites. *Acta Materialia*, 46(4), 1209-1220.
- [16] Zhang, J., Perez, R.J., Gupta, M., & Lavernia, E.J. (1993). Damping behavior of particulate reinforced 2519 Al metal matrix composites. *Scripta Metallurgica et Materialia*, 28(1), 91-96.
- [17] Ersulu S.O., & Aydogdu M, Mechanical and Vibration analysis of Al/SiC composite plates. Ankara International Aerospace Conference AIAC-070 (2007).
- [18] El-Kady, E. Y., Mahmoud, T. S., El-Betar, A. A., & Abdel-Aziz, M. (2012). Dynamic behaviour of Cast A356/Al<sub>2</sub>O<sub>3</sub> aluminum metal matrix nano composites. *Materials Sciences and Applications*. 3(11), 815-820.
- [19] Ravikanth Raju, P., & Venkat Reddy, R. (2018). Mechanical characterization and free vibration of composite laminated plates. *International Journal of Mechanical Engineering and Technology (IJMET)* 9(9), 186-191.
- [20] Soleymani Shishvan, S., & Asghari, A. H. (2017). Effects of particle shape and size distribution on particle size-dependent flow strengthening in metal matrix composites. *Scientia Iranica B*, 24 (3), 1091-1099.
- [21] Civalek, Ö., Numanoğlu, H. M., & Mercan, K. (2019). Finite element model and size dependent stability analysis of boron nitride and silicon carbide nanowires/nanotubes. *Scientia Iranica*, 26(4), 2079-2099.
- [22] Khan, A.A., Naushad Alam, M., & Wajid, M. (2016). Finite element modelling for static and free vibration response of functionally graded beam. *Latin American Journal of Solids and Structures*, 13, 690-714.
- [23] Zuo, H., Yang, Z., Chen, X., Xie, Y., & Zhang, X. (2014). Bending, free vibration and buckling analysis of functionally graded plates via wavelet finite element method. *Computers, Materials and Continua (CMC)*, 44 (3), 167-204.
- [24] An, X., Liu, Y., Huang, F., & Jia, Q. (2018). MPFEM modeling on the compaction of Al/SiC composite powders with core/shell structure. *Powder Technol.* DOI: 10.5772/IntechOpen.76563, pp. 21-43, (2018).
- [25] Bozkurt, Y., & Ersoy, S. (2016). Determining the vibration behavior of metal matrix composite used in aerospace industry by FEM. *Vibroengineering PROCEDIA*. 9, 29-32.
- [26] Santhosh, N., & Kempaiah, U. N. (2018). Vibration characterization of SiCp and fly ash dispersion strengthened

- aluminium 5083 composites. *Journal of Aerospace Engineering & Technology*. 7(3), 61-72.
- [27] Kushwaha, P.K., & Vimal, J. (2014). Study of vibration analysis of laminated composite plates using FEM. *International Journal of Advanced Mechanical Engineering*. 4(6), 675-680.
- [28] Alaneme, K.K., & Fajemisin, A.V. (2018). Evaluation of the damping behaviour of Al-Mg-Si alloy-based composites reinforced with steel, steel and graphite, and silicon carbide particulates. *Engineering Science and Technology, an International Journal*. 21(4), 798-805.
- [29] Gholami, R., & Ansari, R. (2019). On the vibration of postbuckled functionally graded-carbon nanotube reinforced composite annular plates. *Scientia Iranica*, 26(6), 3857-3874.
- [30] Vinyas, M., Sunny, K.K., Harursampath, D., Nguyen-Thoi, T., & Loja, M.A.R. (2019). Influence of interphase on the multi-physics coupled frequency of three-phase smart magneto-electro-elastic composite plates. *Composite Structures*. 226, 111254.
- [31] Vinyas, M., Sandeep, A.S., Nguyen-Thoi, T., Ebrahimi, F., & Duc, D.N. (2019). A finite element-based assessment of free vibration behaviour of circular and annular magneto-electro-elastic plates using higher order shear deformation theory. *Journal of Intelligent Material Systems and Structures*. 30(16), 2478-2501.
- [32] Vinyas, M., Nischith, G., Loja, M.A.R., Ebrahimi, F., & Duc, N.D. (2019). Numerical analysis of the vibration response of skew magneto-electro-elastic plates based on the higher-order shear deformation theory. *Composite Structures*. 214, 132-142.
- [33] Avinash, L., Ram Prabhu, T., & Bontha, S. (2016). The Effect on the dry sliding wear behavior of gravity cast A357 reinforced with dual size silicon carbide particles. *Applied Mechanics and Materials*. 829, 83-89.
- [34] Lakshmikanthan, A., Bontha, S., Krishna, M., Koppad, P. G., & Ramprabhu, T. (2019). Microstructure, mechanical and wear properties of the A357 composites reinforced with dual sized SiC particles. *Journal of Alloys and Compounds*. 786, 570-580.
- [35] Avinash Lakshmikanthan, T. Ram Prabhu, Udayagiri Sai Babu, Praveennath G. Koppad, Manoj Gupta, Munishamaiah Krishna , Srikanth Bontha (2020). The effect of heat treatment on the mechanical and tribological properties of dual size SiC reinforced A357 matrix composites. *Journal of Materials Research and Technology*. 9(3), May June 2020, 6434-6452
- [36] Matweb.com.2020.Matweb-The Online Materials Information Resource.[online] Available at :<<http://www.matweb.com/search/DataSheet.aspx>>
- [37] Mahesh, V., Sagar, P. J., & Kattimani, S. (2018). Influence of coupled fields on free vibration and static behavior of functionally graded magneto-electro-thermo-elastic plate. *Journal of Intelligent Material Systems and Structures*. 29 (7), 1430-1455.
- [38] Herrmann, J., Kühn, T., Müllenstedt, T., Mittelstedt, S., & Mittelstedt, C. (2018). Closed-form approximate solutions for the local buckling behaviour of composite laminated beams based on third order shear deformation theory. *Advances in Mechanics of Materials and Structural Analysis*. 80, 175-205.
- [39] Vinyas, M., Kattimani, S.C. (2018). Finite element evaluation of free vibration characteristics of magneto-electro-elastic plates in hygrothermal environment using higher order shear deformation theory. *Composite Structures*. 202, 1339-1352.
- [40] Vinyas, M. (2018). A higher order free vibration analysis of Carbon Nanotube-reinforced Magneto-electro-elastic plates using finite element methods. *Composites Part-B*. 158, 286-301.
- [41] Mohammadimehr, M., Okhravi, S.V. & Akhavan Alavi, S.M. (2018). Free vibration analysis of magneto-electro-elastic cylindrical composite panel reinforced by various distributions of CNTs with considering open and closed circuits boundary conditions based on FSDT. *Journal of Vibration and Control*. 24(8), 1551-1569.
- [42] Shen, H.S. (2009). Nonlinear bending of functionally graded carbon nanotube-reinforced composite plates in thermal environments. *Composite Structures*. 91, 9-19.
- [43] Klimenda, F., & Soukup, J. (2017). Modal analysis of thin aluminium plate. *Procedia Engineering*. 177, 11-16.